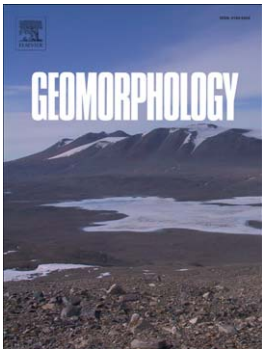

Geomorphological mapping of ice-free areas using polarimetric RADARSAT-2 data on Fildes Peninsula and Ardley Island, Antarctica

T. Schmid, J. López-Martínez, S. Guillaso, E. Serrano, O. D'Hondt, M. Koch, A. Nieto, T. O'Neill, S. Mink, J.J. Durán, A. Maestro

PII: S0169-555X(16)30881-9
DOI: doi: 10.1016/j.geomorph.2016.09.031
Reference: GEOMOR 5778

To appear in: *Geomorphology*

Received date: 27 May 2015
Revised date: 11 September 2016
Accepted date: 16 September 2016

Please cite this article as: Schmid, T., López-Martínez, J., Guillaso, S., Serrano, E., D'Hondt, O., Koch, M., Nieto, A., O'Neill, T., Mink, S., Durán, J.J., Maestro, A., Geomorphological mapping of ice-free areas using polarimetric RADARSAT-2 data on Fildes Peninsula and Ardley Island, Antarctica, *Geomorphology* (2016), doi: 10.1016/j.geomorph.2016.09.031

Geomorphological mapping of ice-free areas using polarimetric RADARSAT-2 data on Fildes Peninsula and Ardley Island, Antarctica

T. Schmid[1], J. López-Martínez[2], S. Guillaso[3], E. Serrano[4], O. D'Hondt[3], M. Koch[5], A. Nieto[2], T. O'Neill[6], S. Mink[2,7], J. J. Durán[7], A. Maestro[2,7],

[1]CIEMAT, Avda. Complutense 40, 28040 Madrid, Spain, thomas.schmid@ciemat.es (corresponding autor)
[2]Dpto. Geología y Geoquímica, Facultad de Ciencias, Universidad Autónoma de Madrid, 28049 Madrid, Spain, jeronimo.lopez@uam.es, s.mink@igme.es
[3]Computer Vision and Remote Sensing Group, Technische Universität Berlin, Office MAR 6-5, Marchstr. 23, Berlin, Germany, stephane.guillaso@tu-berlin.de
[4]Dpt. Geografía, Universidad de Valladolid, Paseo Prado de la Magdalena s/n, 47011 Valladolid, Spain, serranoe@fyl.uva.es
[5]Center for Remote Sensing, Boston University, Boston, MA, USA, mkoch@bu.edu
[6]School of Science, Waikato University, Hamilton, New Zealand, toneill@waikato.ac.nz
[7]Instituto Geológico y Minero de España, Ríos Rosas, 23, 28003 Madrid, Spain, jj.duran@igme.es; a.maestro@igme.es

Abstract

Satellite-borne Synthetic Aperture Radar (SAR) has been used for characterizing and mapping in two relevant ice-free areas in the South Shetland Islands. The objective has been to identify and characterize land surface covers that mainly include periglacial and glacial landforms, using fully polarimetric SAR C band RADARSAT-2 data, on Fildes Peninsula that forms part of King George Island, and Ardley Island. Polarimetric parameters obtained from the SAR data, a selection of field based training and validation sites and a supervised classification approach, using the support vector machine were chosen to determine the spatial distribution of the different landforms. Eight periglacial and glacial landforms were characterised according to their scattering mechanisms using a set of 48 polarimetric parameters. The mapping of the most representative surface covers included colluvial deposits, stone fields and pavements, patterned grounds, glacial till and rock outcrops, lakes and glacier ice. The overall accuracy of the results was estimated at 81%, a significant value when mapping areas that are within isolated regions where access is limited. Periglacial surface covers such as stone fields and pavements occupy 25% and patterned grounds over 20% of the ice-

free areas. These are results that form the basis for an extensive monitoring of the ice-free areas throughout the northern Antarctic Peninsula region.

Keywords: Periglacial, RADARSAT-2, polarimetry, geomorphology, ice-free areas, South Shetland Islands.

1. Introduction

The largest warming trends recorded in Antarctica have been on the western and northern parts of the Antarctic Peninsula over the past sixty years (Turner et al., 2014). In the case of the South Shetland Islands, the ice-covered area of King George Island has decreased by 1.6% during 2000– 2008 (Ruckamp et al., 2011). Therefore, glaciers and snow fields are retreating and the permafrost is thawing. This leads to changes in surface hydrology and affects ecosystems (Moreno et al., 2012; López-Martínez et al., 2016).

It is well known that Antarctic terrestrial ecosystems develop under extreme conditions and are vulnerable to environmental change (Convey, 2010; Cowan, 2014). Alterations in the regional climate, especially the oscillations around the freezing point of water , cause important changes in biological activity, chemical and physical weathering, regional hydrology and geomorphic processes (Michel et al., 2014a). Periglacial environments are frequently marginal to the glaciers, and are subject to cycles of freezing and thawing. The presence of permafrost and its associated processes, when the ground temperature remains at or below 0ºC for at least two consecutive years, is closely associated with the periglacial environment (Dobinski, 2011) Most of the ice-free ground in Antarctica is underlain by frozen ground (Guglielmin, 2012). In contrast, paraglacial processes, landforms and landscapes are those that are directly conditioned

by former glaciation and deglaciation (Ballantyne, 2002). Therefore, periglacial, paraglacial and permafrost processes and related landforms are among the most relevant geomorphological features in the ice-free areas of the northern Antarctic Peninsula region. These feature and processes are closely related to the hydrological cycle, affecting the surface and underground water circulation (Moreno et al., 2012) and the ecosystems within the mentioned areas. Furthermore, in the studied region, soils and landforms are also affected by physical weathering and cryogenic processes, especially by freeze-thaw cycles and the presence of permafrost (López-Martínez et al., 2012). Most of the studies on the periglacial environment in the region of interest have been dedicated to patterned ground, gelifluction, cryoclastic and cryoturbation processes, and permafrost and active layer (John and Sudgen, 1973; Barsch et al., 1985; Vtyurina and Moskalevskiya, 1985; Xie, 1988; Cui et al., 1989; Qingsong, 1989; Zhu et al., 1996; Serrano and López-Martínez, 2000, 2012; Jeong, 2006; Serrano et al., 2008, López-Martínez et al., 2012). There are further initial studies focussed on soils and cryogenic processes (Chen and Blume, 1999; Chen et al. 2000). During the last ten years a considerable amount of soil, permafrost and geomorphological studies have been carried out in the northern Antarctic Peninsula region which is becoming warmer and more moist (Michel et al., 2006, 2012, 2014b; Navas et al., 2006, 2008; Simas et al., 2006, 2007, 2008; Schaefer et al., 2007; Serrano et al., 2008; Vieira et al., 2008, 2010; Francelino et al., 2011; López-Martínez et al., 2012; Moura et al., 2012; Balks et al., 2013; Bockheim et al., 2013). The relationship between landforms and soil distribution in Antarctica has been addressed in a comprehensive study (Balks et al., 2013) as well as the distribution and changes of vegetation related to permafrost warming (Guglielmin et al., 2014; Vieira et al., 2014).

Ice-free areas in the South Shetland Islands are marked by paraglacial and periglacial processes and landforms (López-Martínez et al., 2012), which influence soil development as well as vegetation distribution (Cannone and Guglielmin, 2010). Topography, soil characteristics, vegetation, slope orientation and geomorphology are seen as major factors affecting permafrost occurrence and distribution (Michel et al., 2012, 2014b).

Acquiring field data in the harsh environment of the Antarctic Peninsula region is a logistical challenge in many cases. Therefore remote sensing is ideally suited to the region and offers a great potential to identify relief and landscape features as well as changes in areas for which little or no data are available. Studies carried out in Antarctica use different sensors that operate in the optical and microwave range (Magagi and Bernier, 2003; Vieira et al., 2014). However, the frequently dense cloud cover in Maritime Antarctica limits the application of optical sensors, so that microwave sensors can be the most appropriate option (Schmid et al., 2012; Mora et al., 2013). The use of Synthetic Aperture Radar (SAR) images has been implemented in numerous studies for terrain mapping (Grunsky, 2002; Pavlic et al., 2008), and permafrost mapping (Li and Guo, 2000; Longépé et al., 2009) including within the Antarctic region (Engeset and Weydahl, 1998; Jezek, 1999; Jezek et al., 2003; Koch et al., 2008, 2009; Schmid et al., 2012). The use of fully polarimetric information from SAR data increases the ability to interpret and analyze different soil states and relate these to the physical properties of the scattering behaviour on the ground. This behaviour is due to the dielectric properties of the soil or surface cover (Mironov et al., 2005). Developments of space-borne SAR sensors such as ALOS PALSAR and RADARSAT-2, with fully polarimetric options, have opened up further possibilities for the extraction of information associated with permafrost, glacial and geological surface structures as well

as the shoreline of islands in the Antarctic region (Koch et al., 2008; Van der Sanden, 2004). Polarimetric RADARSAT-2 C-band data have been used to determine soil freezing and thawing states, even under distinct dry snow cover (Jagdhuber et al., 2014). Research work has been published to illustrate the surface mapping capabilities of RADARSAT-2 and its potential for global exploration applications within the Antarctic region (Scheuchl et al., 2012; Schmid et al., 2012). This has also been shown by the RADARSAT-2 Antarctica mosaic that was acquired during 2008 (Hillman et al., 2011). The landscape of ice-free regions within the South Shetland Islands is influenced by the geological morphostructure and the deglaciation history (Mink et al., 2014, 2015). Periglacial processes are important in these regions where land surface covers are under the influence of freeze-thaw cycling effects. These contribute to a complex distribution of surface features and influence soil development and vegetation distribution that are closely related to their abiotic and biotic characteristics (Guglielmin, 2012; Guglielmin and Vieira, 2014). Due to natural changes and anthropogenic influences related to climate change and the increasing activities of scientific studies, the characterisation of the land surface covers that comprise the fragile ecosystems is crucial for the management and conservation of terrestrial ecosystems. In this case, satellite data and spatial data analysis are ideal tools to detect and quantify the land surface cover distribution within remote areas with limited access, and also to identify possible future changes.

The objective of this study is to identify and characterize land surface covers that include periglacial and paraglacial landforms with fully polarimetric SAR C band RADARSAT-2 data in the ice-free regions of Fildes Peninsula and Ardley Island within the northern Antarctic Peninsula region. This included field measurements obtained during several campaigns, in which were studied the most representative surface covers,

extracting information from polarimetric data, and using an additional geomorphological map database to associate the different surface covers with identified landforms.

2. Study area

Fildes Peninsula and Ardley Island are located in the Southwestern end of King George Island (approx. 62º 11´S-58º 58´W), in the South Shetland Islands, Western Antarctica (Fig. 1a and b). Ardley Island is to the Southeast of the peninsula and the closest points between the peninsula and the island are approximately 400 m apart. The peninsula and the island, with extensions of 29 km^2 and 1.2 km^2, respectively, account for the most extensively snow-free coastal areas in summer on King George Island, most of which is permanently covered by ice. The peninsula is separated at its tip from Nelson Island by Fildes Strait, which is only 370 m wide at its narrowest. It is bounded on its Southeast coast by Maxwell Bay, also known as Fildes Bay, and on its Northwest by the open waters of the Drake Passage (Fig. 1b and c). Four scientific stations and one airport are located on the peninsula that is limited by the Collins Glacier to the North (Fig. 1d).

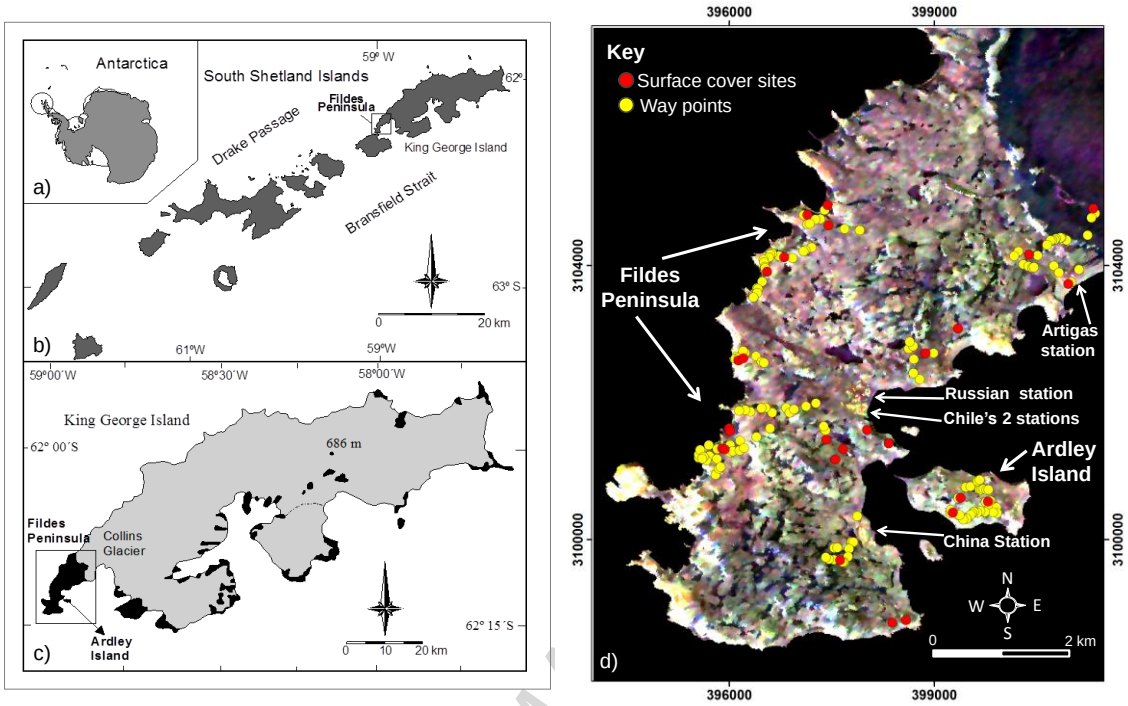

Fig. 1. The study area a) in Antarctica within the b) South Shetland Islands, on the c) Southwestern tip of King George Island and d) colour composition using elements of the coherency matrix (HH-VV, HV and HH+VV) according to the Pauli decomposition, shows Fildes Peninsula and Ardley Island data using full polarimetric RADARSAT-2 satellite data (© MacDONALD, DETTWILER AND ASSOCIATES LTD. 2009 – All Rights Reserved).

The climate of Fildes Peninsula is cold maritime, with daily summer temperatures that can be higher than 0º C (Rakusa-Suszczewski, 2002). A mean annual temperature of -2.2ºC at 10 m a.s.l. has been recorded in Fildes Peninsula in the period 2000-2012 (Michel et al., 2014a), The average annual precipitation is 687.4 mm for the years 1969 to 2005 (AARI, 2006) and the annual average wind speed is 7.34 m s^{-1}, which are high throughout the year and reach their highest levels from March to October (Peter et al., 2008). During summer the total snow cover melts and there are around 122 potential freeze –thaw cycles per year. The summer precipitation, the relative air humidity (80-90%), and the snow melt imply high summer water availability to soils and sediments.

Two high lands of 142 and 139 m a.s.l. respectively, are located in the central portion of the peninsula and a central depression of E-W direction (where the airport and the Chilean and Russian stations are located). The ice-free area is mainly occupied by Early Tertiary to Quaternary volcanic rocks outcropping basaltic, andesite and dacite lavas, agglomerates, lapillistone and tuffs (Smellie et al., 1984). The main geomorphic features in Fildes Peninsula and Ardley Island are periglacial, glacial and coastal ones. Main coastal landforms were generated by interaction between sea action and tectonic uplift, forming a relief characterised by wide platforms, mainly to the Northwest and West side mostly comprising the Middle platforms, located between 30-50 m a.s.l. The Upper platforms, located at 100-150 m form small platforms scattered in the South and the Northeast sectors. Finally, under the palaeocliffs of the Middle platforms and slopes are located a series of raised beaches of Holocene age. Existing radiocarbon dates and relative sea-level curves from raised beach and lake sediments for Fildes Peninsula indicate that the uppermost elevated beach dates to ~9000-7000 cal. a B.P. although some data from stratigraphic sections and lake cores suggest a deglaciation as early as ~9500 cal. B.P. (Hall, 2010; Watcham et al., 2011). Fildes Peninsula was shaped by glaciers during the Pleistocene and part of the Holocene, and glacial landforms are dominant on the North and South highlands with more than 100 lakes generated in glacial overdeepened basins. Later on, small coalescent icefields occupied the emerged lands, occupying the fjords. Maxwell Bay was ice-free at ~5.9 ka and the Fildes deglaciation occurred between 8-5 ka B.P. (Mäusbacher et al., 1989; Simms et al., 2011); a period when the periglacial processes and landforms began to be the most important ones.

The geomorphological map (Fig. 2)) show a distribution of the main periglacial, glacial and marine features.

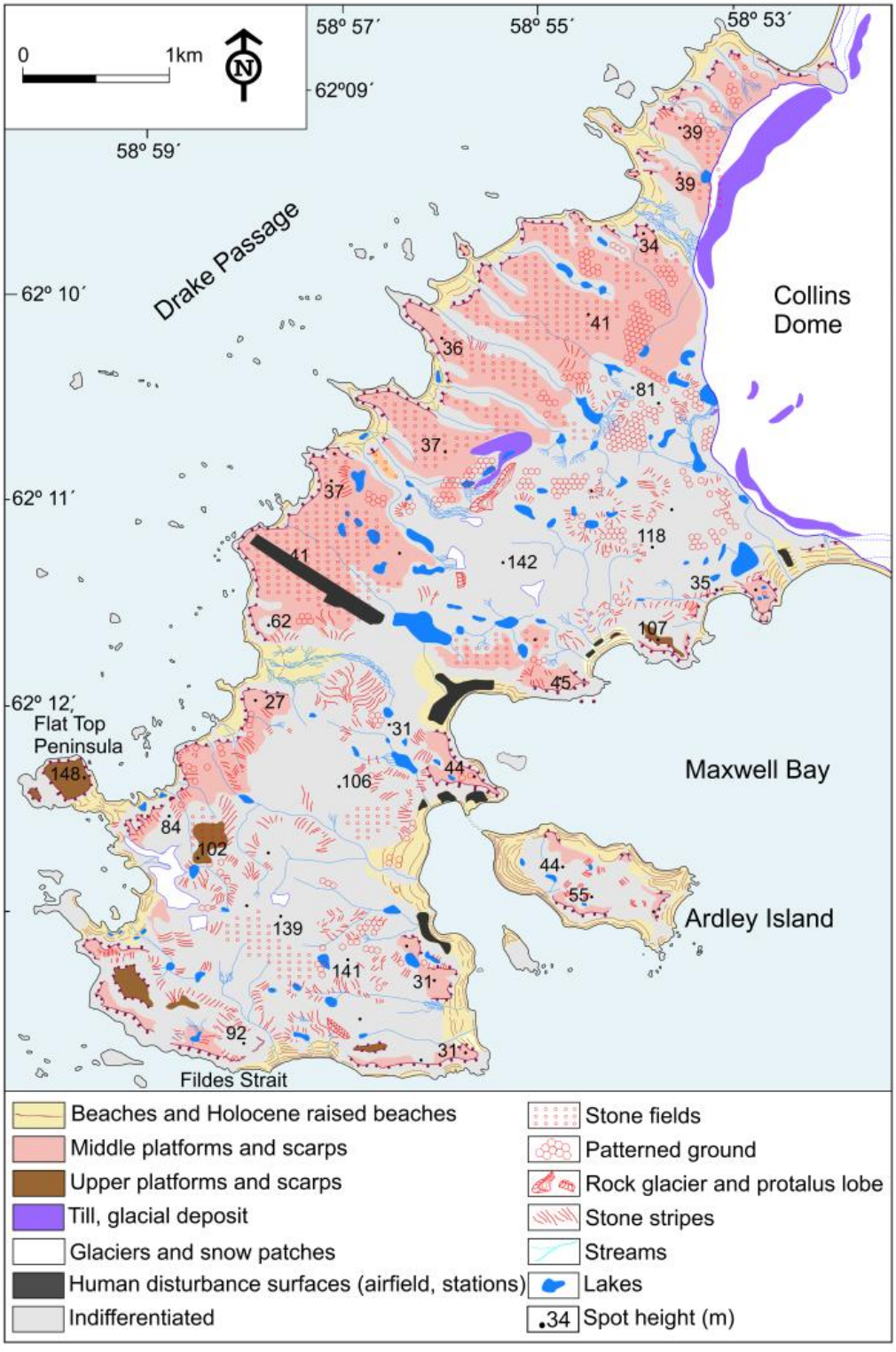

Fig. 2. Geomorphological map of Fildes Peninsula and Ardley Island (Simplified version from Serrano and López-Martínez, 2012).

The presence of permafrost and periglacial processes on Fildes Peninsula and Ardley Island are strongly linked. The active periglacial landforms occupy around one third of the total surface of the peninsula, and are mainly located on the raised platforms of marine origin above 30-50 m a.s.l., where cryoturbation is the main process. On the Holocene raised beaches and low to moderate platforms there is a low to moderate periglacial activity, and this is the domain of nival processes. Only a few periglacial features exist at low altitudes (0-20 m a.s.l.), but they are dominant above 50 m a.s.l. At low altitudes (0-20 m a.s.l.) there are no features linked to permafrost, and under palaeocliffs and structural scarps debris talus and cones are dominant. Snow pavements, sandur, asymmetrical valleys and flat floored valleys, are common on flat and slope areas.

The amount and type of terrestrial vegetation depend on relief, soil moisture content, and the degree of soil enrichment from birds and seals. The region is home to two flowering plants - Antarctic hair grass (*Deschampsia antarctica*) and Antarctic pearlwort (*Colobanthus quitensis*). Some areas are densely covered by moss carpets. A total of about 175 lichen and 40 moss species have been identified in the studied area (Peter et al., 2008).

3. Methods

An outline of the method applied for this study (Fig. 3), was carried out using different data sources. This included detailed field data obtained during the 2012-2013campaign, which served to obtain georeferenced surface cover data, soil and sediment samples, as well as to determine *in situ* observations of the different processes and forms that are present. Data and thematic maps representing the geomorphology, lithology and

geology that were acquired and produced in former field campaigns (López-Martínez et al., 2012) were also implemented. Remotely sensed Synthetic Aperture Radar (SAR) data that cover the entire region of Fildes Peninsula and Ardley Island were acquired by the Canadian Space Agency on the 8th of March 2014 with the spaceborne RADARSAT-2 (C-Band). This is a fully polarimetric single look complex (SLC) dataset taken with an average incidence angle of 40º and a ground resolution of 4.98 m (azimuth) by 7.34 m (range).

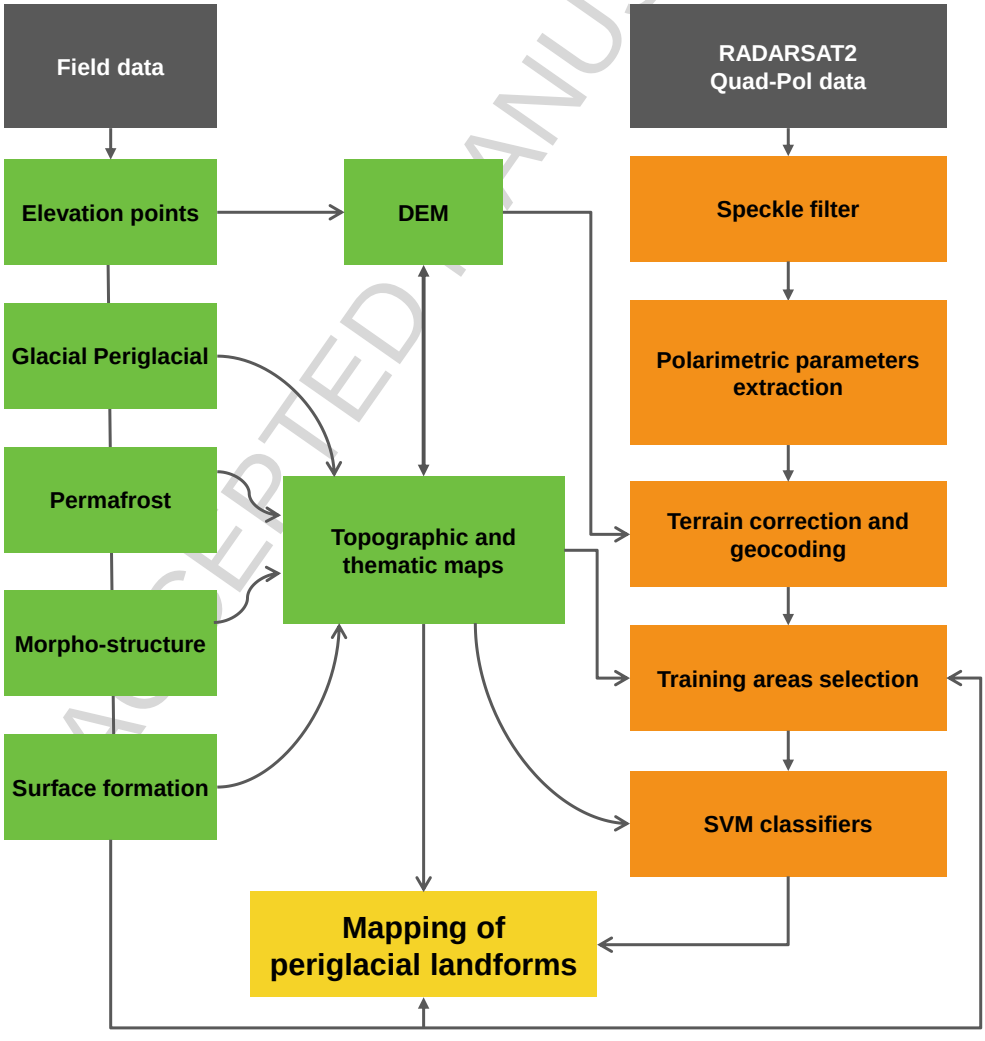

Fig. 3. Method applied to map periglacial and associated landforms.

3.1. Field data

During the campaign (2012-2013) the work was focused on obtaining field data (Fig. 4) that was used both to train and validate the classifier model and results obtained using the SAR imagery data. A total of 27 study plots and 138 waypoints were selected for the different surface covers.

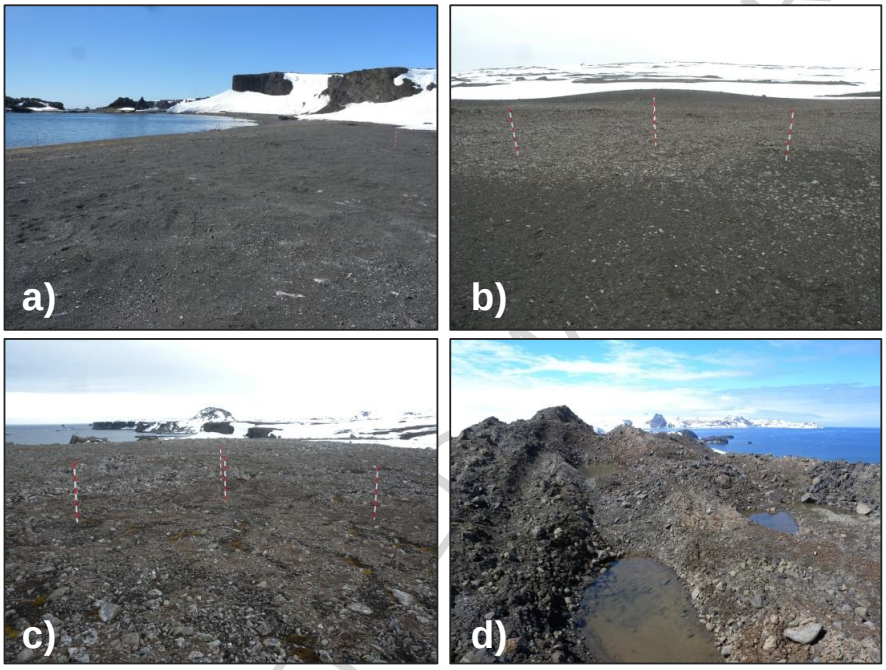

Fig. 4. Surface characteristics related to a) beach (class 1); b) stone cover (class2), c) patterned ground (class3) and d) glacial till (class 4).

The study plots were selected sites with an extension that was adapted to the spatial resolution of the SAR image and where detailed observations as well as samples were obtained (Fig. 5). Further georeferenced waypoints also represented surface areas where observations were taken, however no sampling was carried out.

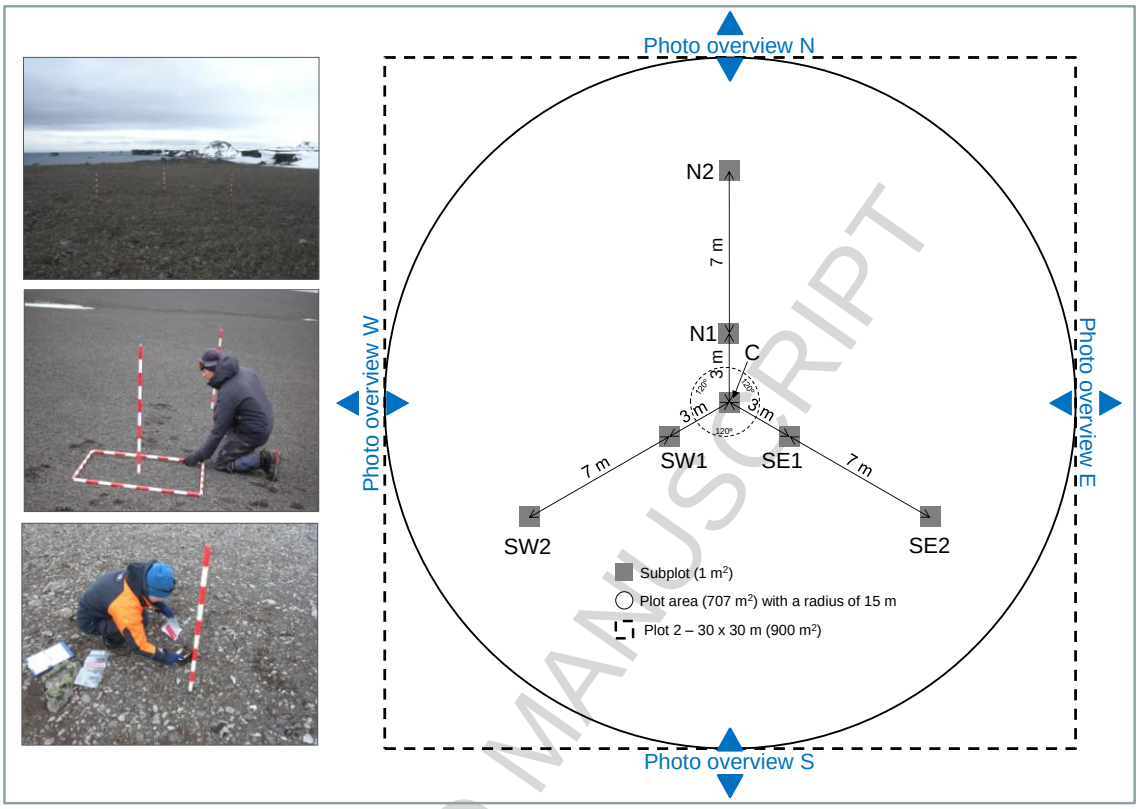

Fig. 5. Field plot area with corresponding sub-plots.

The plot area A (m²) of a single plot was determined taking into account the pixel size P (m) of the SAR sensor and the geometric accuracy (pixels) according to Justice and Townshend (1981):

$$A = (P\,(1 + 2G))^2 \quad (1)$$

The spatial resolution after the pre-processing of the RADARSAT-2 is a minimum of 10 m. Therefore, considering an area of 30 by 30 m (3 by 3 pixels), the total area calculated with equation 1 is 900 m^2. A simplified set up of the field plots was carried out using a survey pole, tape measure and compass (Schmid et al., 2016), where 7 subplots, each of 1 m^2, are located within an circle using a central point C and situating the N, SE and SW subplots a distance of 3 m and 10 m from the centre, respectively, with an angle of 120° between the corresponding subplots. This configuration is a

tradeoff between representing the surface cover and time spent in the field setting up the plot. Field observations for each plot (estimating stone–size and cover, vegetation cover) and surrounding area were characterized. Soil and sediment samples were taken in the field and analysed in the laboratory.

3.2. Cartographic management

Field data were processed and compiled into a georeferenced database using a Geographical Information System (GIS) of all the generated data. GIS techniques were applied to create support layers containing information for the different thematic maps. Data contained as a topographic map were used to create a digital elevation model (DEM) that was used for the geometric correction of the SAR data. The DEM grid was prepared using the 'Topo to Raster' tool from ArcGIS 10.1 software (ESRI, 2013). Source data used as input for the raster processing tool included contour lines (contour interval 5 m), point elevation and hydrological information (streams and lakes) from the topographical map at a scale 1:10,000 of Fildes Peninsula (Instituto Geográfico Militar, 1996).

3.3. Polarimetric SAR data preparation

The fully polarimetric SAR data file was extracted and each polarimetric image is stacked into a so-called scatering vector, meaning that each pixel of the image is represented by a vector. Then a polarimetric calibration and symmetrisation was carried out before a conversion of each scatering vector into a complex (3x3) coherency matrix (T3) which needs to be statistically estimated by first using an image size reduction of a factor 2x2 (summing 2 lines and 2 columns) and then by applying a speckle filter called Polarimetric SAR Bilateral Filter (PolSAR-BLF) (D'Hondt et al., 2013) in order to

reduce speckle effect and to allow a better estimation of different polarimetric features, derived from the analysis of the coherency matrix (Lee and Pottier, 2009).For each pixel of the image, a matrix is extracted and an eigendecomposition is carried out, given a set of 3 eigenvalues and 3 eigenvectors. Then, the different polarimetric parameters are extracted from the eigenvalues and eigenvectors (Lee and Pottier, 2009).

Table 1: Polarimetric parameters extracted from the H/A/Alpha decomposition (Cloude and Pottier, 1996; Lee and Pottier, 2009)

Polarimetric Parameters extracted from the H/A/Alpha decomposition		
Alpha (α_1, α_2, α_3)	Beta (β_1, β_2, β_3)	Gamma (γ_1, γ_2, γ_3)
Delta (δ_1, δ_2, δ_3)	Entropy (H)	Anisotropy (A)
Combination Entropy/Anisotropy	Anisotropy12	Asymetry
Entropy Shannon Intensiy/Polarity	Gini Simpson Index	Index qualitative variation
Inverse Simpson Index	Pseudo probability (p_1, p_2, p_3)	Pedestal
Perplexity	Polarisation Fraction	Rényi_Entropy (2, 3, 4)
Radar Vegetation Index	SERD, DERD	Shannon/Simpson Index
Element of the coherency matrix T (9 parameters)		

A total of 48 parameters were determined (Table 1) with the PolSARpro program (Pottier, 2010): Entropy (H) which measures the degree of randomness of the scattering process; the Anisotropy (A) which indicates the relative importance of the lowest eigenvalues; combinations between Entropy and Anisotropy (HA, H[1-A], [1-H]A, [1-H][1-A]); the Single bounce Eigenvalue Relative Difference (SERD) and the Double bounce Eigenvalue Relative Difference (DERD) which are related to the characterization of natural surface. Furthermore, the Shannon Entropy ($SE = SE_I + SE_P$)

which corresponds to the contribution related to intensity (SE_I) and polarimetry (SE_P) (Morio et al., 2008); the Polarization Asymmetry (PA) and the Polarization Fraction (PF) which give information about the distribution of the total power over the different polarimetric channels; the Radar Vegetation Index (RVI) which gives information about the natural target randomness; the Pedestal Height (PH) which also measures the randomness degree in the scattering process and the anisotropy 12 (A12) which is similar to the A but over the highest eigenvalues. Moreover, different diversity indices have also been calculated (Jost, 2006): Gini Simpson Index; Shannon Index; Rényi Entropy; Simpson Index; Inverse Simpson Index; Index Qualitative Variation and Perplexity. From the eigenvectors, different parameters (α_1, α_2, α_3, β_1, β_2, β_3, δ_1, δ_2, δ_3, γ_1, γ_2, γ_3) are used to define the target polarization orientation angle (the subscripts are indicating which eigenvectors is taken into consideration: 1 means dominant scatterer, 3 corresponds to the less dominant scatterer). The mean α angle is also be related to the type of scattering mechanisms (SMs): $\alpha = 0°$ means surface scattering, $\alpha = 90°$ means a double bounce scattering, typically due to ground wall interactions in man-made areas. Furthermore, the normalized form of the eigenvalues (p_1, p_2, p_3) and the values of the coherency matrix (T) were used with the following 9 parameters: T11, Re(T12), Im(T12), Re(T13), Im(T13), T22, Re(T23), Im(T23), T33). All of these parameters are useful to understand the different SMs that occurred during data acquisition, using fully polarimetric SAR image.

Thereafter, georeferencing of the coherency matrix and decomposition parameters was carried out to associate the backscattering information with the geomorphological features according to the field data and reference maps mentioned above. This included geocoding and terrain corrections that were carried with respect to a DEM with a spatial resolution of 10 m using the Sentinel-1 Toolbox (S1TBX, 2014). A final geometric

correction was applied with 20 GCPs taken from the topographical map at a scale 1:10,000 of Fildes Peninsula (Instituto Geografico Militar, 1996). The level of accuracy of the georeferencing was determined with a root mean square error of 0.46 and the final spatial image resolution was 12.5 m. A mask was applied to eliminate the sea surrounding the peninsula before carrying out further image processing.

3.4. Supervised classification

The supervised Support Vector Machine (SVM) classifier (Foody and Mathur, 2004a) was used to categorize the different surface covers related to the periglacial environment into several classes according to the different polarimetric features. The SVM classifier is a standard classifier that was considered the best option because of its good performance when the amount of training data is limited (Foody and Mathur, 2004b) and achieves good results even with small training data sets (Melgani and Bruzzone, 2004). In this case, the SVM is based on the Gaussian Radial Basis Function (RBF) kernel from the e1071 package (Meyer et al., 2016) implemented in the R language (R Development Core Team, 2004) was used. The input data set was made up of the 48 polarimetric decomposition parameters that were stacked and scaled to a range of 0-1. The scaling was carried out to avoid attributes in greater numeric ranges dominating those in smaller numeric ranges, thus biasing the results (Hsu et al., 2010). A selection of training sites representing 8 classes, which could be well separated by the corresponding SMs with the RADARSAT-2data, was used in the SVM classifier. For each class, between 8 to 14 training sites (minimum number if pixels per training site was 2) that accounted for a total of 81 sites with a total area of 35156 m^2 (225 pixels) were selected for the supervised classification according to the following criteria: 1) Field data from different test sites and the geomorphological map of Fildes Peninsula

(Serrano and López-Martínez, 2012) were chosen to obtain training areas that correspond to specific geomorphological units, 2) interpreting backscattering mechanisms obtained from the different training areas according to the different polarimetric parameters, and 3) combining polarimetric parameters such as H and A to improve the capability to distinguish the different types of scattering processes. Training sites (Fig. 4) were chosen within areas that covered an average of 3 by 3 pixels (30 by 30 m) (Fig. 5) corresponding to the spatial resolution of the fine polarimetric image obtained with RADARSAT-2 . These training sites were used to train the SVM classifier. Applying a 10-fold cross-validation on the training data, a penalty parameter C of 8192 and a gamma parameter of $1.953125e^{-3}$were determined with a total accuracy of 88%.

Thereafter a validation was carried out using a confusion matrix to obtain the overall accuracies, estimation of the Kappa coefficient, individual class accuracies as well as producer's and user's accuracy (Congalton, 1991). A separate set of ground truth sites were used to assess the confidence with which the classification was made. These sites were selected according to reference points acquired *in situ*. A total of 95 validation sites were obtained for all the classes. Further sites were determined according to data sources from maps (López-Martínez et al., 2012; Serrano and López-Martínez, 2012) and from remotely sensed optical sensors (Landsat and SPOT). The size of the sites to be considered were found within areas that were at least 3 by 3 pixels in size

4. Results and discussion

A total of 8 classes were differentiated according to 48 polarimetric parameters that were used (Table 1). An example of some of the polarimetric parameters that were used in this work (Fig. 6) show that individual SMs can be associated to different surface cover features that were identified in the ground truth data.

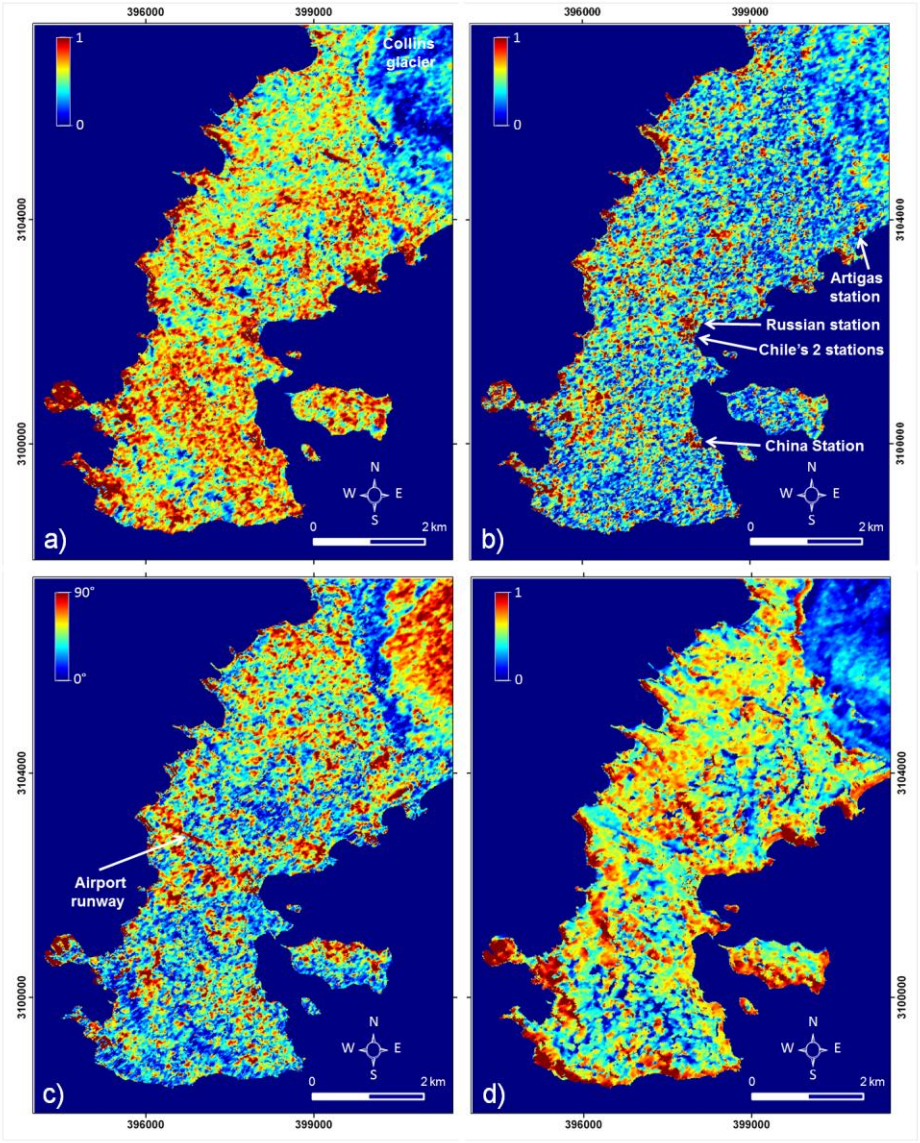

Fig. 6. Polarimetric parameters a) H, b) HA, c) α_1 and d) SE_I.

H (Fig. 6a) represents randomness of scattering and is a measure of the dominance of a given SM for each pixel. H shows the randomness of a scattering medium from isotropic scattering (H=0) to totally random scattering (H=1). Values in between indicate the degree of dominance of one particular scatterer. Low H values are significant in the Northern part of Fildes Peninsula on Collins Glacier and areas where water bodies and snow cover are encountered. The A is a measure of the difference between the secondary SMs and cannot be interpreted separately from the entropy. A possible combination between H and A, denominated as HA (Fig. 6b) is associated to

two dominant SMs. Therefore high values of HA correspond to two SM that show abrupt changes in the terrain such as cliffs and rock outcrops, and where large boulders are found within the glacial till. Futhermore, the different research stations (Chile's Base Presidente Eduardo Frei Montalva and Professor Julio Escudero Base, China's Great Wall Station, Russia's Bellingshausen Station and Uruguay's Artigas Base) can be well identified due to the SMs produced by the buildings. The α angle (Fig. 6c) identifies the dominant SM present in the object. In this case the α_1 parameter indicates the SM that is associated with the first eigenvector. The α_1 values that are lower than 45° correspond to surface scattering and are related to the water bodies and water saturated areas. According to the meteorological conditions on Fildes Peninsula 8 days (1^{st} to 8^{th} of March 2014) prior to the image data acquisition, there was a total of 63.5 mm of rainfall (WMO, 2014). On the day of acquisition (8^{th} of March 2014, 23:52) there was continuous weak to moderate rainfall (9 mm). This means that the surface covers were wet influencing the backscattering signal that the radar sensor receives. The SE_I (Fig. 6d) contribution depends on the total backscattering power. Low values are associated to water bodies, snow and ice cover. Intermediate values are related to the distribution of patterned ground, pavements and stone fields characterized by moderate volume scattering. High values are related to the glacial till and rock outcrops where strong SMs occur due to the abrupt changes in terrain surfaces.

Training sites were selected according to the type of SM and were related to the corresponding characteristics. These included physical properties such as geomorphological features, associated topography, physical properties such as texture and structure of the terrain surface, and the type of Radar SM (Table 2). The Radar SM is key to separate and map the different surface cover features. This approach is good to retrieve very different SMs that identify contrasting structures and processes, but becomes challenging when there is a lack of contrasting surface covers.

Table 2. Description of training site classes selected for the supervised classification.

Class	Geomorphological features	Topography	Physical properties	Radar Scattering Mechanism (SM)
1	Gravel and sand deposits of present day and Holocene beaches, colluvium deposits	Mainly in flat and depression regions (<2%) as well as the toeslope where material is deposited	Coarse sediments to rounded pebble sized stones	Low to medium entropy and high anisotropy. Surface and volume SM
2	Stone cover	In flat, slightly sloping areas (<2%) and undulating terrain	A surface cover of stones (10-50 cm) and fractured rocks.	Low to medium entropy, low anisotropy. Surface

		(2-8%)		and volume SM
3	Patterned ground	Flat or undulating topography with maximum slope reaching <30%	Geometric (hexagons or circles) figures with 1 to 3 m diameter, a sorted distribution and clasts up to about 30 cm	High entropy and low anisotropy. Random SM
4	Glacial till deposits and rock out crops	Crests separated by depressions, abrupt changes with steep slopes (> 30%), and cliffs	Ice cored moraine sediments with varying rock size and exposed rock surfaces with debris slopes at the footslope	Medium and high entropy volume and multiple scattering
5	Ice and snow cover	Flat or undulating topography with maximum slope reaching <30%	Smooth surface of ice or snow cover. Very season dependent	Low to medium entropy. Surface SM
6	Exposed glacier ice with sediments and larger accumulation of ice	Slightly sloping to steep slopes	Rough surface with abrupt changes such as crevices or broken ice blocks with possible deposit of sediments	Medium and high entropy. Surface and volume SM
7	Lakes and flooded regions	Flat surface found from sea level to the upper platforms	Very smooth feature. Unstable in windy conditions.	Low entropy with surface SM
8	Surface cover influenced by vegetation	Flat to steep surfaces (< 30%)	Smooth to coarse surface with partial or total humid vegetation cover of moss and lichens	Low to medium entropy. Surface SM

The classes represent the principal geomorphological features; however it is likely that certain features will be represented by more than one class. This is the case for classes 1 to 3 where the physical surface variation of the surface materials and their distribution over a small area for these classes can vary significantly. The surfaces such as glacial till and rock out crops (class 4) and ice and snow cover (class 5) and lakes and flooded regions (class 7) have well defined SMs. The classes of exposed glacier ice with irregular structure and sediment accumulation, and surface covers such as stone fields and patterned grounds that may well be influenced by vegetation such as mosses and lichens, have a heterogeneous physical structure which again influence the backscattering of the electromagnetic radiation received by the RADARSAT-2 sensors. The vegetation cover can be made up of a sparse cover containing lichens and/or moss to a thick coating of moss that may cover entire surface structures as is common on Ardley Island and on present day and Holocene beaches.

The distributions of the 8 classes were obtained for the land surface area and occupied a total surface area of 33 km^2 (Fig. 7).

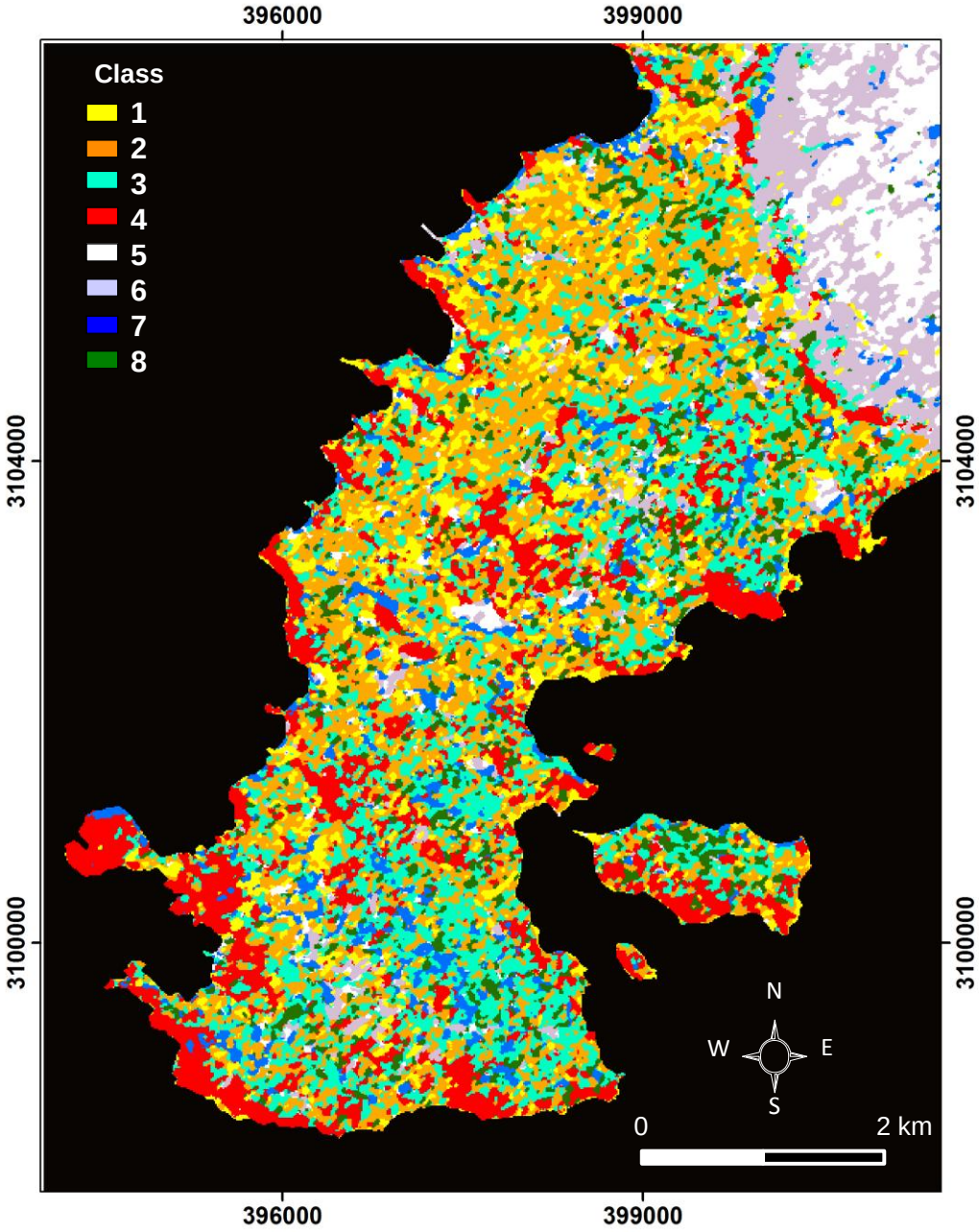

Fig. 7. Supervised classification of the geomorphological features on Fildes Peninsula and Ardley Island.

The distribution of the gravel and sand deposits of present day and Holocene beaches, and colluvium deposits (class 1) occupy an area of 3.2 km^2 (9.6%). As expected, colluvium deposits are found throughout the region. The drainage areas are the prime

location for these types of deposits. The stone cover surface (class 2) that include both pavements and stone fields occupy the largest distribution of 8.25 km^2 (25%). Stone fields are very common above 30 m a.s.l., mainly on the Middle platforms (30-50 m a.s.l.) where poor drainage and permafrost are dominant. In the raised platforms with flat topography, between 20 and 100 m a.s.l., the poor drainage on the platforms and the snow cover melt during summer produce an optimal environment for stone field and patterned ground development, with an increase of patterned ground with altitude. Patterned ground extensions (class 3) have been identified over a total of 6.7 km^2 (20.3%). This coverage is coherent with the geomorphological map (Fig. 2) where it is estimated that patterned ground, including polygons, stone stripes and circles, are the most common periglacial landforms in Fildes Peninsula (López-Martínez et al., 2012 Serrano and López-Martínez, 2012). These landforms are mainly located above 60 m a.s.l. and are dominant above 90 m a.s.l. They occur wherever landscape stability, clayey substrate and poor drainage are present to sustain moist content (Michel et al., 2014b). On the North and South Highlands of Fildes Peninsula, circles and stone stripes are the most common periglacial features occupying wide extensions of small glacial overdeepened basins, slopes and higher platforms. Slopes are the domain of gelifluction processes, forming landforms linked to permafrost, such as protalus lobes and a rock glacier, or landforms such as gelifluction and debris lobes, related to frozen ground, all of which are located mainly at altitudes above 50 m a.s.l. As the physical structure and composition of the surface pavement, stone field and patterned ground are similar; the fine separation of the backscattering for these surfaces is more difficult. Patterned ground can also vary widely in size from sub metric size to tens of meter. Therefore, the capability of the identification of patterned ground with the polarimetric RADARSAT-2 data lies mainly in the size of the surface structure and will range from features with about 10 to 25 m. Smaller or larger patterned ground structures will therefore be related to the class with debris structure that include surface pavement and stone fields.

Glacial till and rock outcrops (class 4) have an important extent of 5.3 km^2 (16%). These features are well defined at the Collins Glacier front and deposits of the retreating glacier in the past. Rock outcrops are found at different locations within the central part of the peninsula and the island as well as at numerous locations around the coast where abrupt cliffs form the raised platforms above 90 m. The common characteristics of these features are the size of the physical structure (> 10 m) and the abrupt surface changes.

These can include boulders, massive igneous bodies, scarps and crests of hills that may have sizeable crevices and clefts. In this case SMs are well identified in the Radar data due to the abrupt changes of these big surface structures.

The surface covers associated with ice and snow (class 5) and exposed glacier ice with loose sediment cover and affected by surface changes such as crevices (class 6) are 2.4 km^2 (7.2%) and 3 km^2 (4.2%), respectively. The former class has a smooth surface with ice formation mainly on the upper part of Collins Glacier and on water bodies as well as snow cover that depends largely on the meteorological conditions. The latter class represents exposed compact ice that forms part of the glacier front with crevices and as protruding ice masses in water bodies. Furthermore, on the lower slopes of the glacier, the ice can also be sparsely covered with rock debris and sediments. The distribution of the water bodies and flooded regions (class 7) are 1.9 km^2 (5.8%) and has the least extent of all the classes. These are smooth surfaces with a low entropy surface scattering and are well identified. The lakes are often delineated by steep scarps and rock outcrops. The final class where surface covers are influenced by vegetation (class 8) has an extent of 2.4 km^2 (7.3%) with important areas found on Ardley Island, along the coast as well as along the borders of streams and rivers. Although it is the second smallest extent, it is significant as vegetation cover in this region is sparse and consists mainly of lichens, moss and Antarctic hair grass and pearlwort. The areas with an important vegetation cover are Antarctic Specially Protected Areas (ASPA) which are of special scientific interest and contain a rich biodiversity (Fildes Peninsula - ASPA125 and Ardley Island – ASPA150). Classes 5 and 7 are closely related to the meteorological conditions and will have an important effect on being able to determine the geomorphological surface covers when they are flooded or lie under an extensive snow cover.

A confusion matrix (Table 3) was established with 95 validation points. The overall accuracy obtained for the data was 81% with a Kappa coefficient of 0.78. These values are considered to have a relatively high accuracy (given the difficulty of the classification scenario) and have been obtained for the different classes within a complex mosaic of processes that influence the study region.

Table 3. Confusion matrix of the supervised SVM classification showing the producer and user accuracy.

Class	Ground truth validation sites (%) 1	2	3	4	5	6	7	8	Total (%)	Prod. Acc. (%)	User Acc. (%)
1	83.3	7	0	0	0	0	0	8.3	12.6	83.3	83.3
2	16.7	78.6	16.7	7.7	0	0	0	8.3	17.9	78.6	64.7
3	0	7.1	75.0	0	0	0	0	8.3	11.6	75.0	81.8
4	0	7.1	0	92.3	0	0	0	0	13.7	92.3	92.3
5	0	0	0	0	90.0	20	16.7	0	13.7	90.0	69.2
6	0	0	0	0	10.0	80.0	0	0	9.5	80.0	88.9
7	0	0	0	0	0	0	83.3	8.3	11.6	83.3	90.9
8	0	0	8.3	0	0	0	0	66.7	9.5	66.7	88.9
Total (%):	100.0	100.0	100.0	100.0	100.0	100.0	100.0	100.0	100.0		

The producer's accuracy for individual classes of the different surface covers varies between 66.7% (class 8) and 92.3% (class 4) indicating how well a certain class is classified. The user's accuracy varies between 64.7% (class 2) and 92.3% (class 4) indicating the probability that the pixel classified on the image actually represents that class. In general the different surface covers are well classified. Most confusions are easily explained and are logical regarding the complex mosaic of the surface properties.

In general, the classes have high producer and user accuracy and therefore, their distribution can be well determined throughout the area. Even classes where certain confusion can occur, such as 1, 2 and 3, have a moderate percentage as wrongly classified. Classes 1 and 3 have a confusion of 16.7 % with class 2 in both cases. This means that beach areas of colluvial deposits may contain rock and stone fractions that are recognized in the class of stone cover. Or the class of patterned ground can be confused with the stone covers. This is especially the case when patterned grounds are not well defined or are influenced by surface movement due to water flow or vegetation expanding in the area. This amount of confusion between the classes is considered reasonable, as there are sometimes small differences regarding the back scattering properties. Class 2 was confused with class 3 and 4 representing patterned ground and

glacial till deposits and rock out crops.. Again there are similarities in the physical structure such as surface roughness and stone size. Class 8 is confused with a number of the other classes such as colluvial deposits, stone covers, patterned ground water saturated areas. Therefore, the vegetation class is shown to cover different land cover surfaces that are stable. Class 6 and class 7 representing exposed glacier ice with the accumulation of sediments and water surfaces are shown to be confused with snow and ice cover. In the former case, this is due to areas where debris covering the ice is not so dense and in the latter case, open water surfaces are frequently covered by ice

It is clear that Fildes Peninsula and Ardley Island have important topographic variations with abrupt changes represented by large surface features such as glacial till with boulders, escarpments and cliffs as well as depressions left from the influence of past glacial activities. These surfaces have multiple SMs that stand out from the rest of the land surface covers. The same applies to the smooth surfaces with low entropy and surface SMs such as water bodies, ice and snow cover. Different raised platforms, especially along the Western half of Fildes Peninsula have large extensions were periglacial features such as area covered by stones representing stone fields and pavements, and patterned ground are dominant. The result of glacier oscillations and consequent receding of Collins Glacier to the present position has left an undulating topography with numerous depressions and an extended network of drainage channels. As a result, there is a heterogeneous mosaic of surface covers that are related to the different SMs that can be identified by polarimetric SAR images such as fully polarimetric RADARSAT-2 data.

It has to be regarded that the work carried out with the polarimetric Radarsat-2 data has provided a qualitative interpretation of the polarimetric parameters of the different surface covers. Although contrasting surfaces between glacial till and rock out crops,

the stone covers and smooth surfaces such as lakes are well interpreted. However, more small changes in the structure and composition of surface covers would need data of higher spatial resolution.

Within the pre-processing chain of the polarimetric data there are a series of important issues to address, which include the application of the polarimetric speckle filter. In this case, so called texture information can be lost if the filter is not applied with the correct limits set to obtain the optimal information from the data. Furthermore, the geometric correction of the data is a further important step, to be able to associate external data to the SAR data. It is essential to have a good set of ground truth data as training sites for the supervised classifier as well as for the validation of the results. A careful selection of the training sites representing the chosen classes is time consuming and needs a thorough knowledge of the geomorphological processes that influence the surface structure of the different land surface covers. The field methodology in this work made it possible to separate the main surface cover features. Although features such as the class of stone covers representing surface pavement and stone fields and the class patterned ground, as well as to some extent the gravel and sand deposits, can vary greatly and often subtle changes in their physical composition is what separates them from each other. For these features, it was a challenge to obtain the corresponding information using the RADARSAT-2 data and applying advanced polarimetric techniques for Fildes Peninsula and Ardley Island within the northern Antarctic Peninsula region.

5. Conclusions

This paper has evaluated the use of fully polarimetric RADARSAT-2 data and processing techniques to successfully characterize the periglacial ice-free surfaces on

Fildes Peninsula and Ardley Island. This included identifying periglacial and glacial features and determining the spatial distribution of the main land surface covers.

The proposed methodology used the polarimetric RADARSAT-2 data within a region where ample field and cartographic data were available. This included constructing a georeferenced data base with all the available data for the pre-processing and processing steps to improve the extraction of information from the acquired SAR data.

The coherency matrix T3, polarimetric parameters extracted from the H/A/α decomposition and the supervised SVM classifier were considered as a robust combination to determine the spatial distribution of the different geomorphological surface covers. Key was to have a set of field based training and validation sites to differentiate the classes representing different surface covers influenced by periglacial processes as well as associated landforms. Classes with smooth surfaces as well as those influenced by abrupt changes represented by surface and multiple SMs were identified with a high degree of accuracy. Acceptable results were obtained for the periglacial landforms dominated by surface and volume SMs and are considered as important features representing the ice-free landscape.

These results of characterizing ice-free areas are considered important within a highly dynamic area such as the Antarctic Peninsula region were direct accessibility in the field is often limited. It is anticipated that the utilization of RADARSAT-2 data and the techniques undertaken in this research can be easily extrapolated to other similar regions where the same processes can be studied. Furthermore, these results form the basis for comparisons with any past studies and possible future monitoring with advanced new radar sensors.

Acknowledgements

This work is supported by the Projects CTM2014-57119-R and CTM2011-26372 of the Spanish R&D National Plan. The authors would like to gratefully thank and acknowledge the support of Canadian Space Agency and MDA for providing the satellite data by means of the Science and Operational Applications Research Program (SOAR) projects SOAR-1376 and SOAR-5169. Furthermore, the authors thank the Spanish logistic personnel and the support provided by the Chilean Antarctic Programme. The contribution of two anonymous referees, that has contributed to improve the manuscript, is also acknowledged.

References

AARI, 2006. Federal Program "World Ocean", Subprogram "Antarctic Research and Investigation", Russian Antarcic Expedition, 2006. Arctic and Antarctic Research Institute (AARI). Online. http://www.aari.aq/default_en.html. Accessed 11 September 2016.

Ballantyne, C.K., 2002. Paraglacial geomorphology. Quaternary Science Reviews, 21, 1935-2017.

Balks, M.R., López-Martínez, J., Goryachkin, S., Mergelov, N., Schaefer, C., Simas, F., Almond, P., Claridge, G.C.G., Mcleod, M., Scarrow, J., 2013. Windows on Antarctic soil landscape relationships: comparison across selected regions of Antarctica. In: Hambrey, M.J., Barker, P.F., Barrett, P.J., Bowman, V., Davies, B., Smellie, J.L., Tranter, M. (Eds.), Antarctic Palaeoenvironments and Earth-Surface Processes. Geological Society, Special Publications, London, 381, pp. 397-410.

Barsch. D., Blümel, W.D., Flügel, W.A., Mäusbacher, R., Stäblein, G., Zick, W., 1985. Untersuchungen zum Periglazial auf der König-Georg-Insel Südshetland-

insel/Antarktika. Deutsche physiogeographische Forschungen in der Antarktis. Bericht über die Kampagne 1983/84. Reports on Polar Research, nº24. Alfred Wegener Institute, Bremenhaven, Germany, 75 p.

Bockheim, J.G., Vieira, G., Ramos, M., López-Martínez, J., Serrano, E., Guglielmin, M., Wihelm, K., Nieuwendam, A. 2013. Climate Warming and Permafrost Dynamics on the Antarctic Peninsula Region. Global and Planetary Change 100, 215-223.

Cannone, N., Guglielmin, M., 2010. Relationships between periglacial features and vegetation development in Victoria Land, continental Antarctica. Antarctic Science 22, 703-713

Chen, J., Blume, H.P., 1999. Study on the Dynamics of Soil Moisture in an Ice-Free Area of the Fildes Peninsula, King George Island, the Maritime Antarctic. Polarforschung 66, 11-18.

Chen, J., Zitong, G., Blume, H.P., 2000. Soils of Fildes Peninsula, King George Island, the maritime Antarctic. Part 1, formation processes and pedogenetic particularities. Chinese Journal of Polar Science 11, 25-38.

Cloude, S.R., Pottier, E., 1996. A review of target decomposition theorems in radar polarimetry. IEEE Transaction on Geoscience and Remote Sensing, 34, 498-518.

Congalton, R.G., 1991. A review of assessing the accuracy of classifications of remotely sensed data. Remote Sens. Environ. 37, 35-46.

Convey, P., 2010. Terrestrial biodiversity in Antarctica - Recent advances and future challenges. Polar Science 4, 135-147.

Cowan, D.A., 2014. Antarctic Terrestrial microbiology. Springer-Verlag Berlin, 328 p.

Cui, Z., Youyu, X., Gengnian, L., 1989. Antarctic periglacial environment and the formation mechanism of "sorted circles" in the Península Fildes. Proccedings

International Symposium on Antarctic Research, Chinese Committe on Antarctic Research, Chinese Ocean Press, Beijing, pp. 82-90.

D'Hondt, O., Guillaso, S., Hellwich, O., 2013. Iterative bilateral filtering of polarimetric SAR data. IEEE Journal of Selected Topics in Applied Earth Observations and Remote Sensing 6, 1628-1639.

Dobinski, W., 2011. Permafrost. Earth-Science Reviews, 108, 158-169.

Engeset, R.V., Weydahl, D.J., 1998. Analysis of glaciers and geomorphology on Svalbard using multitemporal ERS-1 SAR images. IEEE Trans. Geosci. Remote Sens. 36, 1879-1887.

ESRI, 2013. ArcGis 10.2 Redlands, Environmental Systems Research Institute Inc., California, USA.

Foody, G.M., Mathur, A., 2004a. A relative evaluation of multiclass image classification by support vector machines. IEEE Trans. Geosci. Remote Sensing 42, 1336-1343.

Foody, G., Mathur, A., 2004b. Toward intelligent training of supervised image classifications: directing training data acquisition for SVM classification. Remote Sens. Environ. 93, 107-117.

Francelino, M.R., Schaefer, C.E.G.R., Simas, F.N.B., Filho, E.I.F., de Souza, J.J.L.L., Costa, L.M., 2011. Geomorphology and soils distribution under paraglacial conditions in an ice-free area of Admiralty Bay, King George Island, Antarctica. Catena 85, 194-204.

Grunsky, E.C., 2002. The use of multi-beam Radarsat-1 for terrain mapping, Geospatial Theory, Processing and Applications ISPRS Commission IV, Symposium 2002 Ottawa, Canada, 6 p.

Guglielmin, M., 2012. Advances in permafrost and periglacial research in Antarctica: A review. Geomorphology 155-156, 1-6.

Guglielmin, M., Vieira, G., 2014. Permafrost and periglacial research in Antarctica: New results and perspectives. Geomorphology, 225, pp. 1-3.

Guglielmin, M., Dalle Fratte, M., Cannone, N., 2014. Permafrost warming and vegetation changes in continental Antarctica. Environmental Research Letters, 9, 045001, 14 pp.

Hall, B.L., 2010. Holocene relative sea-level changes and ice fluctuations in the South Shetland Islands. Global and Planetary Change 74, 15-26.

Hillman, A., Rolland, P., Chabot, M., Périard, R., Ledantec, P., Martens, N., 2011. RADARSAT-2 Mission Operations Status. IGARSS, pp. 3480-3483.

Hsu, C.W. Chang, C.C., Lin, C.J., 2010. A practical guide to support vector classification. Department of Computer Science, National Taiwan University, Taipei 106, Taiwan. Online: Online: http://www.csie.ntu.edu.tw/~cjlin/libsvm. Accessed 11September 2016.

Instituto Geográfico Militar, 1996. Isla Rey Jorge-Península Fildes. Carta Topográfica, E. 1:10.000. Instituto Geográfico Militar, República de Chile.

Jagdhuber, T., Stockamp, J., Hajnsek, I., Ludwig, R., 2014. Identification of Soil Freezing and Thawing States Using SAR Polarimetry at C-Band. Remote Sens. 6, 2008-2023.

Jeong, G.Y., 2006. Radiocarbon ages of sorted circles on King George Island, South Shetland Island, West Antarctica. Antarctic Science 18, 265-270.

Jezek, K.C., 1999. Glaciological properties of the Antarctic ice sheet from RADARSAT 1 synthetic aperture radar imagery, Ann. Glaciol. 29, 286-290.

Jezek, K. C., Farness, K., Carande, R., Wu, X., Labelle-Hamer, N., 2003. RADARSAT 1 synthetic aperture radar observations of Antarctica: Modified Antarctic mapping mission, 2000. Radio Science 38, 8067, MAR 32, pp. 1-7.

John, B.S., Sudgen, D.E., 1973. Raised marine features and phases of glaciation in the South Shetland Islands. British Antarctic Survey Bulletin 24, 45-111.

Jost, L., 2006. Entropy and diversity. Oikos 113, 363-375.

Justice, C.O., Townshend, J.R.G., 1981. Integrating ground data with remote sensing. In: Townshend J.R.G. (Ed.), Terrain analysis and remote sensing, George Allen and Uniwin, London, pp. 38-58.

Koch, M., López-Martínez, J., Schmid, T., Serrano, E., Gumuzzio, J., 2008. Application of ALOS PALSAR for the study of periglacial features related to permafrost within the South Shetland Islands, Western Antarctica. International Geoscience and Remote Sensing Symposium (IGARSS), Boston, USA. IEEE. Vol. 4. pp. 343-346.

Koch, M., López-Martínez, J., Schmid, T., Serrano, E., Gumuzzio, J., 2009. Evaluating the use of ALOS data (microwave and optical) for mapping geomorphological features of selected areas in Livingston Island, South Shetland Islands (West Antarctica). ESA SP-664. Proceedings of ALOS PI 2008 Symposium, Rhodes, Greece. pp. 1-4.

Lee J.S., Pottier E., 2009. Polarimetric radar imaging: from basics to applications. CRC Press Taylor & Francis Group, Boca Raton, 438 p.

Li, Z., Guo, H., 2000. Permafrost Mapping in the Tibet Plateau Using Polarimetric SAR. International Geoscience and Remote Sensing Symposium (IGARSS). Honolulu, Hawaii, USA. IEEE. pp. 2024-2026.

Longépé, N., Tadono, T., Shimada, M., Pottier, E., Allain, S., 2009. Case studies of frozen ground monitoring using PALSAR/ALOS data. International Geoscience and

Remote Sensing Symposium (IGARSS), Cape Town, South Africa. IEEE. Vol. 2, pp. 1020-1023.

López-Martínez, J., Schmid, T., Serrano, E., Mink, S., Nieto, A., Guillaso, S. 2016. Geomorphology and landforms distribution in selected ice-free areas in the South Shetland Islands, Antarctic Northern Peninsula region. Cuadernos de Investigación Geográfica 42, pp. 1-12. Doi: 10.18172/cig.2965

López-Martínez, J., Serrano, E., Schmid, T., Mink, S., Linés, C., 2012. Periglacial processes and landforms in the South Shetland Islands (northern Antarctic Peninsula region). Geomorphology 155-156, 62-79.

Magagi, R., Bernier, M., 2003. Optimal conditions for wet snow detection using RADARSAT SAR data. Remote Sens. Environ. 84, 221-233.

Mäusbacher, R., Muller, J., Munnich, M., Schmidt, R., 1989. Evolution of postglacial sedimentation in Antarctic lakes (King Georges Island). Zeitschrift für Geomorfologi 33, 219-234.

Melgani, F., Bruzzone, L., 2004. Classification of hyperspectral remote sensing images with Support Vector Machines. IEEE Transactions on Geoscience and Remote Sensing 42, 1778-1790.

Meyer, D., Dimitriadou, E., Hornik, K., Weingesse, A., Leisch, F., Chang, C., Lin, C., 2016. e1071: Misc Functions of the Department of Statistics, Probability Theory Group (Formerly: E1071), TU Wien, Version 1.6-6. Online: Available: http://CRAN.R-project.org/. Accessed 11 September 2016.

Michel, R.F.M., Schaefer, C.E.G.R., Dias, L.E., Simas, F.N.B., Melo Benites, V., Sá Mendonça, E., 2006. Ornithogenic Gelisols (Cryosols) from Maritime Antarctica. Soil Sci. Soc. Am. J. 70, 1370.

Michel, R.F.M., Schaefer, C.E.G.R., Poelking, E.L., Simas, F.N.B., Fernandes, E.I., Bockheim, J.G., 2012. Active layer temperature in two Cryosols from King George Island, Maritime Antarctica. Geomorphology 155-156, 12-19.

Michel, R.F.M., Schaefer, C.E.G.R., López-Martínez, J., Simas, F.N.B., Haus, N. W., Serrano, E., Bockheim, J.G., 2014b. Soils and landforms from Fildes Peninsula and Ardley Island, Maritime Antarctica. Geomorphology 225, 76-86.

Michel, R.F.M., Schaefer, C.E.G.R., Simas, F.M.B., Francelino, M.R., Fernandes-Filho, E.I., Lyra, G.B., Bockheim, J.G., 2014a. Active-layer thermal monitoring on the Fildes Peninsula, King George Island, maritime Antarctica. Solid Earth 5, 1361–1374.

Mink, S., López-Martínez, J., Maestro, A., Garrote, J., Ortega, J.A., Serrano, E., Durán, J.J., Schmid, T., 2014. Insights into deglaciation of the largest ice-free area in the South Shetland Islands (Antarctica) from quantitative analysis of the drainage system. Geomorphology 225, 4-24.

Mink, S., Maestro, A., J. López-Martínez, J., Schmid, T., Galindo-Zaldívar, J., Trouw, R.A.J., 2015. Morphostructural analysis and Cenozoic evolution of Elephant Island, Southern Scotia Arc, Antarctica. International Journal of Earth Sciences 104, 833-851.

Mironov, V.L.; Komarov, S.A.; Li, S.; Romanovsky, V.E., 2005. Freeze-Thaw Processes Radar Remote Sensing: Modeling and Image Processing. IEEE International Symposium on Geoscience and Remote Sensing, Seoul, South Korea, pp. 608–611.

Mora, C., Vieira, G., Ramos, M., 2013. Evaluation of Envisat ASAR IMP imagery for snow mapping at varying spatial resolution (Deception Island, South Shetlands, Antarctica). Antarctic Paleoenvironments and Earth Surface Processes. Geological Society of London, Special Publication, 381, pp. 481-493.

Moreno, L., Silva-Busso, A, López-Martínez, J., Durán, J.J., Martínez-Navarrete, C., Cuchí, J.A., Ermolin, E., 2012. Hydrogeological characteristics at Cape Lamb, Vega Island, Antarctic Peninsula. Antarctic Science 24, 591-607.

Morio, J., Réfrégier, P., Goudail, F., Dubois-Fernandez, P., Dupuis, X., 2008. Information theory-based approach for contrast analysis in polarimetric and/or interferometric SAR images. IEEE Trans. Geosci. Remote Sens., 46, pp. 2185-2196.

Moura, P.A., Francelino, M.R., Schaefer, C.E.G.R., Simas, F.N.B., Mendonça, B.A.F., 2012. Distribution and characterization of soils and landform relationships in Byers Peninsula, Livingston Island, Maritime Antarctica. Geomorphology 155-156, 45-54.

Navas, A., López-Martínez, J., Casas, J., Machín, J., Serrano, E., Durán, J.J., Cuchí, J.A., 2006. Soil characteristics along a transect on raised marine surfaces on Byers Peninsula, South Shetland Islands. In: Fütterer, D.K., Damaske, D., Kleinschmidt, G., Miller, H., Tessensohn, F. (Eds.), Antarctic Contributions to Global Earth Science 8.9. Springer, Berlin–Heildelberg–New York, pp. 467–474.

Navas, A., López-Martínez, J., Casas, J., Machín, J., Durán, J.J., Serrano, E., Cuchí, J.A., Mink, S., 2008. Soil characteristics on varying lithological substrates in the South Shetland Islands, Maritime Antarctica. Geoderma 144, 123-139.

Pavlic, G., Singhroy, V., Duk-Rodkin, A., Alasset, P.J., 2008. Satellite data fusion techniques for terrain and surficial geological mapping. In International Geoscience and Remote Sensing Symposium (IGARSS). Boston, USA, Vol. III, pp. 314-317.

Peter, H.-U., Buesser, C., Mustafa, O., Pfeiffer, S., 2008. Risk assessment for the Fildes Peninsula and Ardley Island, and development of management plans for their designation as Specially Protected or Specially Managed Areas. Umweltbundesamt Research Report 203 13 124, UBA-FB 001155e, Texte 20/08.

Pottier, E. 2010. Recent advances in the development of the open source toolbox for polarimetric and interferometric polarimetric SAR data processing: the PolSARpro

v4.1.5 software. In International Geoscience and Remote Sensing Symposium (IGARSS). Honolulu, Hawaii, USA. IEEE, pp. 2527-2530.

Qingsong, Z., 1989. A comparison of periglacial landforms between the Vestfold Hills, East Antarctica and the Fildes Península of King George Island, west Antarctica. Proccedings International Symposium on Antarctic Research, Chinese Committe on Antarctic Research, Chinean Ocean Press, Beijing, pp. 74-81.

R Development Core Team, 2004. R: A Language and Environment for Statistical Computing. R Foundation for Statistical Computing, Vienna, Austria. Online: http: //www.R-project.org/. Accessed 11 September 2016.

Rakusa-Suszczewski, S., 2002. King George Island-South Shetland Island, Maritime Antarctic. In Beyer L., Bölter, M. (Eds.), Geoecology of Antarctic Ice Free Coastal Landscapes. Springer Verlag, Berlín, pp. 23-40.

Ruckamp, M., Braun, M., Suckro S., Blindow, N., 2011. Observed glacial changes on the King George Island ice cap, Antarctica, in the last decade. Global and Planetary Change 79, 99–109.

S1TBX, 2014. Sentinel-1 Toolbox. Array Systems Computing Inc. and contributers. Online: https://sentinel.esa.int/web/sentinel/toolboxes/sentinel-1. Accessed 11 September 2016.

Schaefer, C.E.G.R., Simas, F.N.B., Gilkes, R.J., Mathison, C., Costa, L.M., 2007. Micromorphology and microchemistry of Cryosols from Maritime Antarctica. Geoderma 144, 104-115.

Scheuchl, B., Mouginot, J., Rignot, E., 2012. Twelve years of ice velocity change in Antarctica observed by RADARSAT-1 and-2 satellite radar interferometry. The Cryosphere Discuss. 6, 1715-1738.

Schmid, T., López-Martínez, J., Koch, M., Maestro, A., Serrano, E., Linés, C., 2012. Geomorphological mapping in the Antarctic Peninsula region applying single and multipolarization RADARSAT-2 data. Can. J. Remote Sensing 38, 367-382.

Schmid, T., Rodríguez-Rastrero, M., Escribano, P., Palacios-Orueta, A Ben-Dor, E., Plaza, A., Milewski, R., Huesca, M., Bracken, A., Cicuéndez, V., Pelayo, M., Chabrillat S., 2016. Characterization of Soil Erosion Indicators Using Hyperspectral Data From a Mediterranean Rainfed Cultivated Region. IEEE Journal of Selected Topics in Applied Earth Observations and Remote Sensing, 9, 845-860.

Serrano, E., López-Martínez, J., 2000. Rock glaciers in the South Shetland Islands, Western Antarctica. Geomorphology 35, 145-162.

Serrano, E., López-Martínez, J., 2012. Geomorphological Mapping in Antarctic Periglacial Environment. The Geomorphological Map of Fildes Península (King George Island, South Shetlands Archipelago). Proceedings of the Tenth International Conference on Permafrost, Volume 4, IPA-Tyumen State Oil and Gas University, Tyumen, Russia, pp. 518-521.

Serrano, E., López-Martínez, J., Cuchí, J.A., Durán, J.J., Mink, S., Navas, A., 2008. Permafrost in the South Shetland Islands (Maritime Antarctica): spatial distribution pattern. In: Kane, D.L., Hindel, K.M. (Eds.), Ninth International Conference on Permafrost, Fairbanks, Alaska. Institute of Northern Engineering, University of Alaska Fairbanks, pp.1621-1625.

Simas, F.N.B., Schaefer, C.E.G.R., Melo, V.F., Guerra, M.B.B., Saunders, M., Gilkes, R.J., 2006. Clay-sized minerals in permafrost-affected soils (Cryosols) from King George Island, Antarctica. Clays Clay Miner. 54, 721-736.

Simas, F.N.B., Schaefer, C.E.G.R., Melo, V.F., Albuquerque-Filho, M.R., Michel, R.F.M., Pereira, V.V., Gomes, M.R.M., Da Costa, L.M., 2007. Ornithogenic Cryosols

from Maritime Antarctica: phosphatization as a soil forming process. Geoderma 138, 191-203.

Simas, F.N.B., Schaefer, C.E.G.R., Albuquerque-Filho, M.R., Francelino,M.R., Fernades-Filho, E.I., Da Costa, L.M., 2008. Genesis, properties and classification of Cryosols fromAdmiralty Bay, Maritime Antarctica. Geoderma 144, 116-122.

Simms A.R., Milliken, K.T., Anderson, J.B., Wellner, J.S., 2011. The marine record of deglaciation of the South Shetland Islands, Antarctica since the Last Glacial Maximum. Quaternary Science Reviews 30, 1583-1601.

Smellie, J.L., Pankhurst, R.J., Thomsom, M.R.A., Davies, R.E.S.,1984. The Geology of the South Shetland Island: VI. Stratigraphy, Geochemistry and Evolution. British Antarctic Survey Scientific Reports, No. 87. British Antarctic Survey, Cambridge, 85 pp.

Turner, J., Barrand, N., Bracegirdle, T., Convey, P., Hodgson, D. A., Jarvis, M., Jenkins, A., Marshall, G., Meredith, M. P., Roscoe, H., Shanklin, J., French, J., Goosse, H., Guglielmin, M., Gutt, J., Jacobs, S., Kennicutt, M. C., Masson-Delmotte, V., Mayewski, P., Navarro, F., Robinson, S. A., Scambos, T., Sparrow, M., Summerhayes, C., Speer, K. & Klepikov, A., 2014. Antarctic climate change and the environment: an update. Polar Record, 50, 237-259.

Van der Sanden, J.J., 2004. Anticipated applications potential of RADARSAT-2 data. Can. J. Remote Sensing 30, 369-379.

Vieira, G., López-Martínez, J., Serrano, E., Ramos, M., 2008. Climate change and permafrost degradation. Geomorphological evidence from Deception and Livingston islands, Maritime Antarctic. In Kane, D.L., Hindel, K.M. (Eds.), Proceedings Ninth International Conference on Permafrost, vol. 2, pp. 1839-1844. Fairbanks, Alaska:

Institute of Northern Engineering, University of Alaska Fairbanks. ISBN 978-0-9800179-3-9.

Vieira, G., Bockheim, J., Guglielmin, M., Balks, M., Andrey, A., Boelhouwers, J., Cannone, N., Ganzer, L., Gilchinsky, D., Goryachkin, S., López-Martínez, J., Meiklejohn, I., Raffi, R., Ramos, M., Schaefer, C., Serrano, E., Simas, F., Sletten, R., Wagner, D., 2010. Thermal state of Antarctic permafrost and active-layer dynamics: Advances during the International Polar Year 2007-2008. Permafrost and Periglacial Processes 21, pp. 182-197.

Vieira, G., Mora, C., Pina, P., Schaefer, C., 2014. A proxy for snow cover and winter ground surface cooling: mapping Usnea sp. communities using high resolution remote sensing imagery (Maritime Antarctica). Geomorphology 225, 69-75.

Vtyurin B. I., Moskalevskiy M. Yu., 1985. Cryogenic landforms on King George Island, South Shetland Islands. Polar Geography and Geology 9, 62-69.

Watcham, E.P., Bentley, M.J., Hodgson, D.A., Roberts, S.J., Fretwell, P.T., Lloyd, J.M., Larter, R.D., Whitehouse, P.L., Leng, M.J., Monien, P., Moreton, S.G., 2011. A new Holocene relative sea level curve for the South Shetland Islands, Antarctica Quaternary Science Reviews 30, 3152-3170. Online: http://rp5.ru/archive.php?wmo_id=89056&lang=es. Accessed 11 September 2016.

WMO, 2014. Estación meteorológica Base Presidente Eduardo Frei Montalva, Antártida, WMO_ID=89056.

Xie, Y., 1988. Chemical weathering in permafrost regions of Antarctica. Great Wall Station of China, Casey Station and Davis Station of Australia. Fifth International Conference, Proceeding, Trondheim, pp. 511-515.

Zhu, C., Cui, Z., Zhang, J., 1996. Relationship between the distributoion of periglacial landforms and glaciation history, Fildes Peninsula, King George Island, Antarctica. Permafrost and Periglacial Processes 7, 95-100.

Highlights:

- Polarimetric RADARSAT-2 data used to map periglacial and glacial landforms.
- A method to characterize ice-free areas in isolated regions with restricted access.
- A total of 8 classes were differentiated according to 48 polarimetric parameters.
- The overall accuracy of the spatial distribution of the landforms is 81%.